Near-infrared image-guided laser ablation of dental decay

You-Chen Tao
Daniel Fried
University of California, San Francisco
San Francisco School of Dentistry
Department of Preventive and Restorative Dental Sciences
707 Parnassus Avenue
San Francisco, California 94143-0758

Abstract. Image-guided laser ablation systems are now feasible for dentistry with the recent development of nondestructive high-contrast imaging modalities such as near-IR (NIR) imaging and optical coherence tomography (OCT) that are capable of discriminating between sound and demineralized dental enamel at the early stages of development. Our objective is to demonstrate that images of demineralized tooth surfaces have sufficient contrast to be used to guide a CO_2 laser for the selective removal of natural and artificial caries lesions. NIR imaging and polarization-sensitive optical coherence tomography (PS-OCT) operating at 1310-nm are used to acquire images of natural lesions on extracted human teeth and highly patterned artificial lesions produced on bovine enamel. NIR and PS-OCT images are analyzed and converted to binary maps designating the areas on the samples to be removed by a CO_2 laser to selectively remove the lesions. Postablation NIR and PS-OCT images confirmed preferential removal of demineralized areas with minimal damage to sound enamel areas. These promising results suggest that NIR and PS-OCT imaging systems can be integrated with a CO_2 laser ablation system for the selective removal of dental caries. [DOI: 10.1117/1.3253390]

Keywords: image-guided ablation; near-infrared; CO_2 laser; demineralization; caries selective ablation; polarization-sensitive optical coherence tomography.

Paper 09321P received Jul. 31, 2009; accepted for publication Aug. 28, 2009; published online Oct. 30, 2009. This paper is a revision of a paper presented at the SPIE conference on Lasers in Dentistry, January 2008, San Jose, California. The paper presented there appears (unrefereed) in SPIE Proceedings Vol. 6843.

1 Introduction

New optical caries imaging systems have been recently developed that are ideally suited to interface with lasers for the selective removal of dental caries. The most promising caries imaging systems employ fluorescence and near-IR imaging methods, including quantitative light fluorescence[1] (QLF), near-IR (NIR) fluorescence,[2] polarization-sensitive optical coherence tomography[3–5] (PS-OCT), and NIR imaging.[4,6,7] These imaging systems can be used for the acquisition of 2-D or even 3-D images of demineralization on tooth surfaces. Lasers have been used for many years for industrial marking and computer-aided design/machining (CAD/CAM), and high-speed scanning systems are in routine use. It is feasible that a similar high-speed computer-controlled scanning system with an integrated compact delivery system can be used to scan a laser over tooth occlusal surfaces to selectively remove either dental caries or composite restorative materials. In previous studies, we demonstrated that lasers can be scanned over tooth surfaces to remove dental composite and pigmented caries using acoustic and spectral feedback to differentiate these materials from sound enamel.[8,9] However, these approaches proved to be unsuccessful for nonpigmented demineralized enamel.[9] In this paper, we have coupled NIR and PS-OCT imaging of simulated and natural caries lesions with a high-speed scanning CO_2 laser ablation system to demonstrate that demineralized enamel can be imaged with high contrast and selectively removed by the laser.

Fluorescence-based caries imaging and detection methods have been under development for more than 20 years and commercial systems such as QLF and the Diagnodent are readily available. Kavo™ (Biberach, Germany) which sells the Diagnodent™ and Er:YAG laser systems has recently introduced an Er:YAG laser hand-piece with an integrated fluorescence feedback system.[10] The operator can monitor the fluorescence signal to determine when all the caries have been removed. Although this is a significant step forward, the primary source of the red fluorescence signal is porphyrin molecules that collect in lesion areas and the concentration of those molecules does not necessarily correlate with the extent of enamel demineralization, particularly for early white spot lesions,[11–13] therefore we believe that other approaches that are more suitable for imaging enamel demineralization are necessary, such as QLF "green fluorescence" or NIR imaging.

At wavelengths past 1300 nm in the NIR, healthy enamel appears transparent and does not strongly scatter light,

Address all correspondence to: Daniel Fried, University of California, San Francisco, San Francisco School of Dentistry, Department of Preventive and Restorative Dental Science, 707 Parnassus Avenue, San Francisco, California 94143-0758. Tel: 415 502 6641; Fax: 415 4760858; E-mail: Daniel.fried@ucsf.edu

1083-3668/2009/14(5)/054045/6/$25.00 © 2009 SPIE

whereas demineralized enamel and carious lesions manifest reduced transmission and strong light scattering, respectively.[14] Therefore, demineralized enamel can be imaged with high contrast for discrimination from healthy enamel. NIR imaging can be used to acquire images of demineralized enamel on proximal and occlusal surfaces, while PS-OCT is capable of acquiring depth-resolved images of demineralization so that tomographic images can be generated. Polarization sensitivity is necessary to remove the strong surface reflections from tooth surfaces for higher contrast images of demineralized areas.[3] These NIR imaging methods can also be used to image demineralized enamel under composite for removal of secondary caries lesions.[5]

Image-guided procedures employing angiography, computed tomography (CT), or magnetic resonance imaging (MRI) are routinely used to acquire preoperative or real-time medical images during treatment to minimize trauma and improve outcomes. A similar approach is feasible for dental surgery exploiting new optical imaging tools and lasers for selective and conservative removal of caries and restorative materials with an emphasis on the preservation of healthy tissue structure. This approach is potentially advantageous for the preparation of the highly vulnerable pits and fissures on the occlusal surfaces prior to the placement of sealants where the laser is well-suited for removing early demineralization, plaque, and debris and opening up the narrow bottlenecks of the fissures. To implement a prototype of an image-guided laser ablation system, we divided the process into three phases: image acquisition, analysis, and treatment. Specifically, we generated binary maps based on NIR and PS-OCT images to guide the CO_2 laser ablation system for the selective removal of areas of demineralization on tooth surfaces. The aim of this study was to test the hypothesis that image-guided laser ablation is feasible for the highly selective removal of dental decay from enamel surfaces with minimal peripheral damage to sound tissues.

2 Materials and Methods

2.1 *Sample Preparation*

Ten $5 \times 5 \times 2$ mm^3, blocks of bovine enamel were prepared from extracted bovine incisors acquired from a slaughterhouse. The samples had a layer of enamel approximately 1 mm thick over a layer of dentin. Surfaces were serially polished with 12-, 9-, and 3-μm embedded diamond polishing discs. A 3×3 grid was cut into the enamel surfaces of the samples to aid in the creation of patterned artificial lesions using a laser (see Figs. 1 and 2). The dimension of the each grid cell was 1.5×1.5 mm^2. Patterned artificial lesions were created by applying a thin layer of acid-resistant varnish to sound enamel areas for protection before submersion in a demineralization solution. Artificial lesions were formed by exposure of the teeth for 9 days to a 40-mL aliquot of an acetate buffer solution containing 2.0 mmol/L calcium, 2.0 mmol/L phosphate, and 0.075 mmol/L acetate maintained at pH 4.9 and a temperature of 37 °C. The demineralization solution produced subsurface lesions to a depth of approximately 100 to 150 μm on the exposed enamel smooth surfaces without loss or erosion of the enamel surface.

Extracted third molar teeth were also collected in the San Francisco bay area with Committee on Human Research (CHR) approval and sterilized by gamma irradiation. Three teeth with visible occlusal lesions were chosen for selective removal in the second part of this study. Small 3-mm-square windows were etched around the lesions using the CO_2 laser to demarcate the area of interest (AOI) to be imaged and subsequently scanned by the laser for selective ablation.

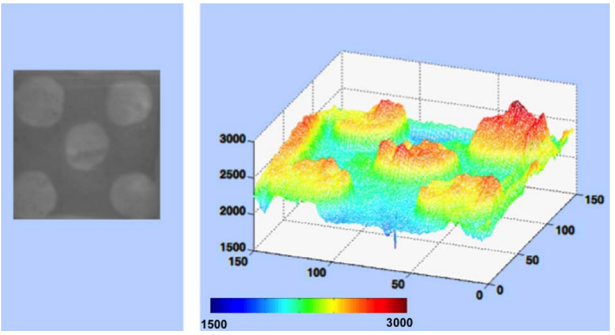

Fig. 1 False color 3-D representation of the grayscale NIR image for one of the patterned lesion (left image) including the threshold determination based on the grayscale level. (Color online only.)

2.2 *NIR Imaging*

Each sample was imaged using the NIR imaging system described in Ref. 15. Light from a 1310-nm superluminescent diode (SLD) with an output power of 15 mW and a 35-nm bandwidth, Model SLED1300D20A (Optospeed, Zurich, Switzerland) was coupled to a 20-mm NIR fiber collimator (Micro Laser Systems, Garden Grove, California). Samples were placed in the 20-mm collimated beam between the light source and imaging system with the enamel side facing the camera. We found that broadband SLDs were advantageous to avoid speckle noise. An InGaAs focal plane array (FPA) (318×252 pixels) the Alpha NIR™ (Indigo Systems, Goleta, California) with an InfinimiteTM video lens (Infinity, Boulder, Colorado) was used to acquire all the images. The acquired 12-bit digital images were analyzed using IRVista™ software (Indigo Systems, Goleta, California). Areas of demineralization appear darker in the NIR images.

2.3 *PS-OCT*

An all single-mode fiber autocorrelator-based optical coherence domain reflectometry (OCDR) system with a polariza-

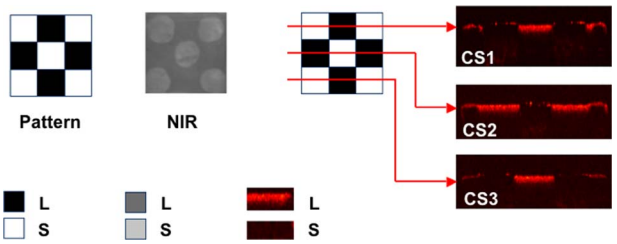

Fig. 2 NIR and PS-OCT images taken of one of the patterned artificial lesions. Three lateral PS-OCT scans "b-scans" or "optical cross sections" (CS) across three different positions are also shown at the respective positions indicated. The PS-OCT scans represent the reflected light in the orthogonal polarization to the original polarization incident on the samples: L, lesion, and S, sound areas.

tion switching probe, high-efficiency piezoelectric fiber stretchers, and an InGaAs receiver that was designed and fabricated by Optiphase, Inc. (Van Nuys, California) was used for these measurements. A description of the scanning autocorrelator is described in Ref. 16. The OCDR was integrated with a broadband high-power SLD (Denselight, Jessup, Maryland) with an output power of 45 mW, a bandwidth of 35 nm, and a high-speed XY-scanning system (ESP 300 controller & 850G-HS stages, Newport, Irvine, California) for *in vitro* optical tomography. Additional details of this system are described in Refs. 16 and 17. Lateral scans, "b-scans," were acquired across either of the patterned artificial lesions or AOI on the extracted human teeth. An electromagnetic Faraday rotator/switch in the probe was used to acquire each of the two polarization states, the incident polarization state and the orthogonal polarization. All the images presented in this paper are of only the orthogonal polarization state. The axial resolution was 22 μm in air and 14 μm in enamel with a lateral resolution of approximately 50 μm over the depth of focus of 10 mm.

2.4 *Ablation Apparatus*

The transverse excited atmospheric pressure (TEA) CO_2 laser (Impact 2500, GSI Lumonics, Rugby, United Kingdom) was operated at a wavelength of 9.3 μm and pulse duration of 16 μs. Tooth samples were irradiated with a fluence of 15 J/cm^2 and an incident energy of 14 mJ per pulse. The laser energy was calibrated and measured using a laser energy/power meter (EPM 1000, Coherent-Molectron, Santa Clara, California) with an ED-200 Joulemeter from Gentec (Quebec, Canada). The laser was focused with a planoconvex ZnSe lens of 100-mm focal length to a beam diameter of approximately 350 μm. The laser beam diameter $(1/e^2)$ at the position of irradiation was determined by scanning with a razor blade across the beam. Two- and three-dimensional images of the laser spatial profile was acquired using a Spirocon Pyrocam™ I pyroelectric array (Logan, Utah). The measured Gaussian laser beam profile suggests that the laser was operated in a single spatial mode. The laser was operated at a repetition rate of 150 Hz and incisions were produced by moving the sample across the beam over spots spaced at 60-μm intervals with each spot receiving 20 pulses. A computer-controlled high-speed XY-scanning system (ESP 300 controller & 850G-HS stages, Newport, Irvine, California) was used to create controlled movement of the samples for the incisions. A low-volume/low-pressure air-actuated fluid spray delivery system consisting of a 780S spray valve, a Valvemate 7040 controller, and a fluid reservoir from EFD, Inc. (East Providence, Rhode Island) was used to provide a uniform spray of fine water mist onto the enamel surfaces at 2 mL/min.

2.5 *Experimental Procedures for Selective Removal*

Selective removal was accomplished in the following sequence: (1) preablation NIR and PS-OCT images were acquired for analysis; (2) those images were converted from 12-bit images to binary maps to control the laser; (3) the laser was scanned to selectively remove lesion areas; and (4) postablation NIR and PS-OCT images were acquired for analysis.

In the first series of measurements, artificial lesions were generated on 10 bovine blocks. Preablation NIR images were captured of the lesion areas, which appeared darker than sound tissue due to decreased transmission of light and increased light scattering at the lesion site. PS-OCT b-scans were acquired at three positions across each including the different variations of each sample pattern. In PS-OCT images, lesion areas manifested higher reflectivity due to the increased light scattering from the areas of demineralization. An image processing module was written using MATLAB (Mathworks, Natick, Massachusetts) to analyze the 12-bit NIR images and set thresholds for distinguishing between sound and demineralized areas. Figure 1 shows one NIR image along with a 3-D graphical representation with the x and y coordinates identifying the position of each pixel and the z coordinate represented by the intensity value of each pixel plotted in false color. Appropriate thresholds were chosen to distinguish between the sound and lesion areas based on the original intensity values. When the z value was less than or equal to the threshold, the tissue was classified as part of the lesion and was demarcated for selective ablation in the treatment phase. If the z value was greater than the threshold, the pixel was marked as sound tissue and was not marked for removal by the laser. The original 12-bit grayscale images were converted to a matrix consisting of pixels spaced 60 μm apart containing binary values, either 0 or 1, demarcating the areas to be ablated using the image processing module.

Another program, written in the Labview™ programming language (National Instruments, Austin, Texas) utilized the binary optical maps to control the laser and scanning system to move the samples across the laser beam. Depending on the value in the optical maps, the laser would either deliver a fixed number of 20 laser pulses at the position of each pixel or scan over that pixel without ablation. Each pixel position was spaced 60 μm apart. After laser ablation, NIR and PS-OCT images were acquired for comparison with the preablation images to assess the selectivity of removal.

Similar steps were taken to remove natural lesions on extracted teeth. Extracted human molars with occlusal caries were selected. A 3×3 mm^2 area of interest enclosing both carious and sound tissue were identified. A box demarcating the AOI was cut into the sample using the CO_2 laser, (see Figs. 5 and 6 in Sec. 3). Preablation NIR and PS-OCT images were captured (see Fig. 6 in Sec. 3). Twenty PS-OCT images were acquired across each sample to provide depth-resolved images of lesion areas. The MATLAB image processing module was used to analyze the 12-bit NIR images to convert the image to a binary map demarcating the sites for ablation by the laser. The number of lasers pulses for the natural lesions was calculated from the PS-OCT scans assuming that each 20 pulses removes 150 μm. Each ablation pixel position was separated by approximately 50 μm apart. Post-ablation visible and NIR images were captured to assess the selectivity of caries removal (see Fig. 5–7 in Sec. 3).

3 Results

Postablation NIR and PS-OCT imaging of the artificial patterned lesions confirmed that lesion areas were removed while sound enamel was conserved with minimal damage to sound tissue. Demineralized areas could be readily differentiated

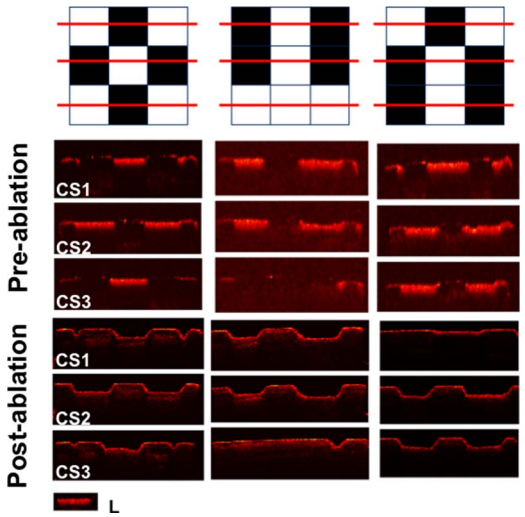

Fig. 3 PS-OCT preablation and postablation images for three of the patterned lesion samples. Scans are shown for each of the different permutations of each pattern. The inset (L) demarcates the appearance of the increased reflectivity in the lesion areas.

from sound areas in the preablation NIR images and the OCT images on all 10 of the samples. This is clearly demonstrated in the images of Figs. 1–4. Figure 1 shows the NIR image of one sample, the lighter areas (round) represent the sound areas while the darker areas represent areas of demineralization. The 3-D graphical representation clearly illustrates that appropriate intensity thresholds can be chosen that demarcate the sound and demineralized areas. Figure 2 shows three PS-OCT b-scans (orthogonal polarization) taken across the sample, as shown in the image presented using a black-red-yellow false color scheme. The lesions areas are visible as intense zones of greater reflectivity approximately 150-μm thick and the PS-OCT images match the patterns extremely well. Figures 3 and 4 show the preablation and postablation PS-OCT and NIR images for 3 and 4 of the 10 samples, respectively. PS-OCT images were acquired at three positions across the patterns to include all permutations of the patterned lesions. The postablation PS-OCT images show that the lesions were removed to a uniform depth and the position of removal matches the position of each lesion area quite well. On one sample, the fourth sample shown in Fig. 4, there was some ablation outside the designated window in the upper right-hand corner, however, that probably occurred due to demineralization in

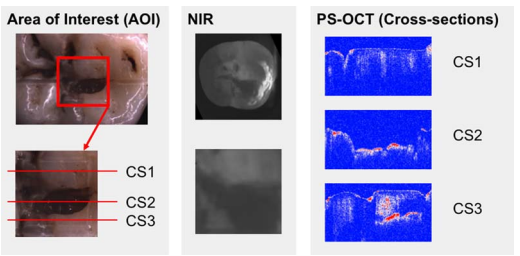

Fig. 5 NIR and PS-OCT images of one of the natural occlusal lesions. Preablation visible and NIR images of the AOI demarcating the area in which selective ablation was carried out are shown. Preablation PS-OCT b-scans are shown for the three positions (CS) across the AOI. Subsurface lesions below sound enamel were observed in the PS-OCT scan, CS3, shown on the lower right.

that area due to leakage through the acid resistant varnish during the demineralization process.

After demonstrating that the artificial lesions patterns could be imaged and selectively ablated, natural occlusal lesions were also investigated on three extracted teeth. Figures. 5–7 show images of occlusal lesions before and after removal. One tooth had a severe occlusal lesion with a region of cavitation and a region of decay hidden below the sound enamel (Figs. 5 and 7). The three optical cross sections (CS) in Fig. 5 correspond to the three PS-OCT b-scans taken across an area of the occlusal surface with a sound area (CS 1), a cavitated area with demineralization (CS 2), and an area of decay below the surface with sound enamel on top (CS 3). The subsurface "hidden" part of the lesion (CS 3 area) is not visible in the visible light image but is visible in the NIR image with high contrast. Visible reflected light images of the occlusal surfaces from each of the three teeth before and after laser ablation are shown in Fig. 6 including the sample shown in Fig. 5. As much as 1.8 mm of enamel was removed from the lesion area of that sample with a mean maximum removal depth of 1.2 mm for each b-scan. The mean removal depths were 0.5 and 0.8 mm, respectively, for the other two samples. Comparing the preablation and postablation images, the results show that selective removal of occlusal caries by combining NIR imaging with a CO_2 laser ablation system is feasible. Most carious tissue was removed, while sound tissues were conserved. Furthermore, this approach can also be used to remove hidden lesions below the sound enamel surface. For example, a large portion of the lesion of Fig. 5 was located under sound enamel, which was clearly evident from the PS-OCT preablation images (CS 3 area). The component of the

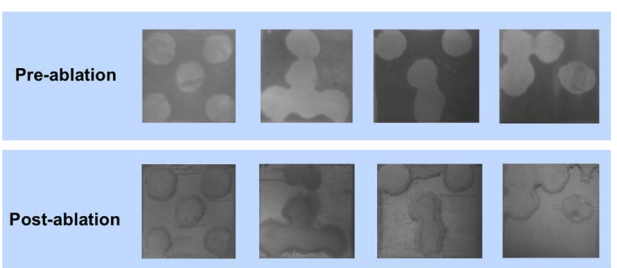

Fig. 4 Near-Infrared (NIR) images of four of the patterned lesion samples before and after laser ablation.

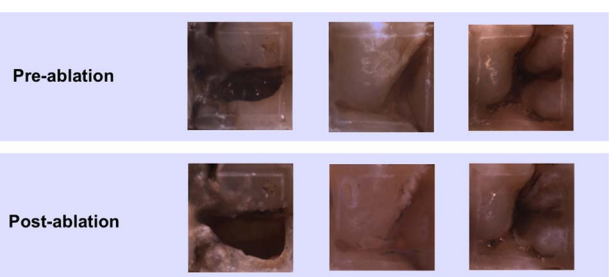

Fig. 6 Preablation and postablation visible reflected light images of the AOI from the three extracted teeth.

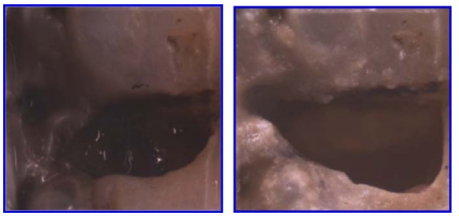

Fig. 7 Closeup view (visible reflected light) of the AOI of the first lesion of Fig. 5, before and after laser ablation.

lesion below the sound enamel was also selectively removed as can be seen in the higher magnification image in Fig. 7. However, we found that multiple passes were required to achieve removal of carious tissue from the designated areas of some of the samples. This was due to either the pooling of the cooling water in the ablation crater or the highly variable state of mineralization of the enamel in the lesions. However, removal was successfully achieved with only one pass for the sample of Fig. 5.

4 Discussion

Postablation NIR and PS-OCT images confirmed that demineralized enamel was selectively removed with minimal damage to sound tissue. This pilot study involving both artificial and natural lesions successfully demonstrated that NIR imaging and PS-OCT can be integrated with a CO_2 laser ablation system for the selective removal of demineralized areas of dental enamel.

In this study, we utilized NIR transillumination imaging and PS-OCT to acquire high-contrast images of artificial and natural caries lesions. Other imaging methods such as green fluorescence based imaging (QLF, 400 to 500-nm excitation) and NIR reflectance imaging may also have sufficient contrast for this approach. In a recent imaging study, we compared the image contrast of artificially demineralized lesions produced on the buccal and occlusal surfaces on whole extracted teeth measured using various imaging methods.[18] NIR reflectance and NIR transillumination were investigated along with QLF (473-nm excitation) and visible reflectance. Crossed polarizers were used to eliminate specular reflection (glare) from tooth surfaces for the NIR and visible light reflectance measurements. NIR transillumination performed poorly for these shallow lesions ($\sim$100 μm deep) due to the large amount of intervening dentin, while NIR reflectance yielded the highest contrast for all the methods investigated and it was the only method that had a significantly higher contrast than visible reflectance measurements.

In this study, the natural lesions on the occlusal surfaces on whole teeth were relatively deep and therefore showed up with high contrast with NIR transillumination. Note that the NIR transillumination of the pits and fissures of the occlusal surfaces does not yield projection type images, that is, the photon paths from the light source to the imager are not necessarily direct or ballistic like an x-ray but that the transparent enamel of the crown is illuminated by the light diffusing upward from the underlying dentin. Two other recent studies involving NIR imaging in the occlusal surfaces shed light on the contrast mechanism and performance, one study involved the NIR imaging of developmental defects,[19] while the other involved multimode reflectance and transmission NIR imaging.[20] These studies confirmed our hypothesis that on whole teeth, only deeper defects or carious lesions show up with high contrast on the occlusal surfaces with transillumination. Moreover, the area and contrast of the occlusal lesions in the NIR transillumination image increase with the depth and severity of the lesion and that these lesion characteristics can be potentially exploited to estimate the severity of the decay. Future NIR/CO_2 laser ablation studies will be carried out using NIR reflectance measurements on smooth surfaces and occlusal surfaces.

The initial results for the natural lesions on whole teeth are promising but indicate the challenges involved in the selective removal of natural caries including overcoming the highly variable topography of the occlusal pits and fissures, the highly variable organic/mineral ratio in natural lesions, and the more complicated lesion structure. Since OCT can yield a measure of the lesion depth, it can also be used to program the depth of removal at each position. However, we found that the caries removal rate varied quite markedly with the severity of demineralization, therefore a more iterative approach that employs multiple passes with repeated imaging between passes is likely to be required. OCT can still be used to provide an endpoint to halt ablation at each position for repeated scans. In a recent development, we have been successful in employing edge detection algorithms for automatic detection of the lesion depth from PS-OCT images.[21] Accurate algorithms for automatic lesion depth calculation should greatly facilitate this approach.

Additional studies are necessary to determine the optimal imaging methods and the best laser parameters for a clinically feasible image-guided ablation system. We found that one advantage of the image-guided approach employing a CO_2 laser is that it is capable of efficiently ablating sound enamel over other methods that require preferential absorption by caries pigmentation and that caries located below sound enamel can be removed, e.g., Fig. 7. Further studies will also explore the real-time tomographic imaging capabilities of OCT.

Acknowledgments

This study was supported by National Institute of Dental and Craniofacial Research (NIDCR) Grants R01 DE19631. The authors would also like to acknowledge the contributions of Cindy L. Darling and Ken Fan.

References

1. U. Hafstroem-Bjoerkman, F. Sundstroem, E. D. J. de Jong, A. Oliveby, and B. Angmar-Mansson, "Comparison of laser fluorescence and longitudinal microradiography for quantitative assessment of *in vitro* enamel caries," *Caries Res.* **26**, 241–247 (1992).
2. R. Hibst, R. Paulus, and A. Lussi, "Detection of occlusal caries by laser fluorescence: basic and clinical investigations," *Med. Laser Appl.* **16**, 205–213 (2001).
3. D. Fried, J. Xie, S. Shafi, J. D. B. Featherstone, T. Breunig, and C. Q. Lee, "Early detection of dental caries and lesion progression with polarization sensitive optical coherence tomography," *J. Biomed. Opt.* **7**(4), 618–627 (2002).
4. R. S. Jones, C. L. Darling, J. D. B. Featherstone, and D. Fried, "Imaging artificial caries on occlusal surfaces with polarization sensitive optical coherence tomography," *Caries Res.* **40**(2), 81–89 (2006).
5. R. S. Jones, M. Staninec, and D. Fried, "Imaging artificial caries under composite sealants and restorations," *J. Biomed. Opt.* **9**(6), 1297–1304 (2004).
6. C. M. Bühler, P. Ngaotheppitak, and D. Fried, "Imaging of occlusal

dental caries (decay) with near-IR light at 1310-nm," *Opt. Express* **13**(2), 573–582 (2005).
7. R. S. Jones, G. D. Huynh, G. C. Jones, and D. Fried, "Near-IR transillumination at 1310-nm for the imaging of early dental caries," *Opt. Express* **11**(18), 2259–2265 (2003).
8. T. M. Louie, R. S. Jones, C. Q. Le, and D. Fried, "Selective removal of composite restorative materials using Q-switched 355-nm laser pulses," *Proc. SPIE* **5313**, 54–60 (2004).
9. J. Y. Cheng, K. Fan, and D. Fried, "Use of a compact fiber optic spectrometer for spectral feedback during the laser ablation of dental hard tissues and restorative materials," *Proc. SPIE* **6137**, 61370F (2006).
10. J. Eberhard, A. K. Eisenbeiss, A. Braun, J. Hedderich, and S. Jepsen, "Evaluation of selective caries removal by a fluorescence feedback-controlled Er:YAG laser *in vitro*," *Caries Res.* **39**(6), 496–504 (2005).
11. A. Lussi and E. Hellwig, "Performance of a new laser fluorescence device for the detection of occlusal caries *in vitro*," *J. Dent.* **34**(7), 467–471 (2006).
12. X. Q. Shi, S. Tranaeus, and B. Angmar-Mansson, "Comparison of QLF and DIAGNOdent for quantification of smooth surface caries," *Caries Res.* **35**(1), 21–26 (2001).
13. S. Tranaeus, L. E. Lindgren, L. Karlsson, and B. Angmar-Mansson, "*In vivo* validity and reliability of IR fluorescence measurements for caries detection and quantification," *Swed Dent. J.* **28**(4), 173–182 (2004).
14. R. S. Jones and D. Fried, "Attenuation of 1310-nm and 1550-nm laser light through sound dental enamel," *Proc. SPIE* **4610**, 187–190 (2002).
15. C. M. Bühler, P. Ngaotheppitak, and D. Fried, "Imaging of occlusal dental caries (decay) with near-IR light at 1310-nm," *Proc. SPIE* **5687**, 125–131 (2005).
16. J. Bush, P. Davis, and M. A. Marcus, "All-fiber optic coherence domain interferometric techniques," *Proc. SPIE* **4204**, 71–80 (2001).
17. P. Ngaotheppitak, C. L. Darling, D. Fried, J. Bush, and S. Bell, "PS-OCT of occlusal and interproximal caries lesions viewed from occlusal surfaces," *Proc. SPIE* **6137**, 61370L (2006).
18. J. I. Wu and D. Fried, "High contrast near-infrared polarized reflectance images of demineralization on tooth buccal and occlusal surfaces at $\lambda = 1310$-nm," *Lasers Surg. Med.* **41**, 208–213 (2009).
19. K. Hirasuna, D. Fried, and C. L. Darling, "Near-infrared imaging of developmental defects in dental enamel," *J. Biomed. Opt.* **13**(4), 044011 (2008).
20. D. Lee, D. Fried, and C. Darling, "Near-IR multimodal imaging of natural occlusal lesions," *Lasers in Dentistry VX*, *Proc. SPIE* **7162**, 71620X (2009).
21. M. H. Le, C. L. Darling, and D. Fried, "Methods for calculating the severity of demineralization on tooth surfaces," *Lasers in Dentistry VX*, *Proc. SPIE* **7162**, 71620U (2009).